

## 4.3 TARGET HEATING DURING INJECTION

The targets contain cryogenic fuel, which must not liquify or vaporize prior to implosion. The targets also have very precise dimensions in their non-fuel shells, which must be maintained prior to irradiation by the driver beams. The required vapor pressure inside the central void of the target is not known, but that pressure is a strong function of the fuel temperature. The purpose of this section is to assess the effects of heating due to radiation from the target chamber walls and due to convective heat transfer from the target chamber gas.

### 4.3.1 Target Conditions

Target designs and heat loads determine the temperatures in the target prior to irradiation by the driver beams. The target designs considered here are representative of future reactor scale targets. Other designs (e.g., different materials or shell thicknesses) may lead to different conclusions. Because there is some uncertainty in the heating rates on the target surfaces, we performed calculations over a range of heat loads.

#### 4.3.1.1 Target Designs

There are two target designs considered in this study: one for direct drive with laser beams (i.e., SOMBRERO) and one for the heavy ion beam driver (i.e., Osiris). Both designs include a low conductivity plastic shell around the cryogenic deuterium-tritium (DT). This shell slows the diffusion of heat from the outside surface of the targets to the cryogenic fuel.

The SOMBRERO target was taken from work performed at the University of Rochester.<sup>4.19</sup> The DT fuel is frozen onto the inside surface of the hollow spherical plastic shell. This frozen DT layer must remain highly uniform until it implodes. The cavity that remains in the center of the DT shell is filled with a very low density DT vapor. The temperature of the fuel must remain low enough that the DT does not melt and distort or that too much DT evaporates and fills the inner cavity. The fuel temperature must certainly remain below the triple point of DT, which is 21 K. With no better information available, we assume 21 K is the temperature limit for the fuel.

We have used the heavy ion target design of Bangerter and others,<sup>4.20</sup> even though this is probably not correct for an indirect-drive target. One difference between the target design used here and that used in other sections of this report is the choice of material for the outer shell. For the target heating calculations we used a lead outer shell. Later in the study, it was determined that tantalum would be a better material for use with Osiris since it is soluble in Flibe. The thermal diffusivities of the two materials at room temperature are very close (0.218 s for tantalum and 0.235 s for lead), so heat transfer will be similar. We assumed that the same

constraints hold for the maximum temperature reached in the DT fuel in the Osiris as in the SOMBRERO target.

#### 4.3.1.2 Heat Loads

We have considered two types of heat loads on the surfaces of both target types; convective heat transfer from the chamber gas to the target and radiative heat transfer from the target chamber walls.

As the target moves through the target chamber gas, heat is absorbed by the surface of the target at a rate that is a function of the target velocity,  $V$ , the mass density of the cavity gas,  $\rho$ , the target diameter,  $D$ , the viscosity of the chamber gas,  $\mu$ , the thermal conductivity of the gas,  $k_f$ , and the temperature difference between the gas and the surface of the target,  $\Delta T$ . The surface conductance for a spherical target with a subsonic velocity is

$$\bar{h}_c = \frac{0.37 R_e^{0.6} k_f}{D}$$

where  $R_e$  is the Reynolds number of the cavity gas,

$$R_e = \frac{V D \rho}{\mu}$$

The surface heating rate in power per unit area is

$$\ddot{q} = \bar{h}_c \Delta T$$

The radiation heat load is assumed to be the black body radiation power produced by a body at the wall temperature  $T_w$ ,

$$\ddot{q}_r = \sigma_s T_w^4$$

where  $\sigma_s$  is the Stefan-Boltzmann constant.

The gas conditions are very different in the two reactor designs. The target velocity for both reactor concepts are in the range of 100 to 200 m/s. The approximate heat loads for the two target are given in Table 4.11. The viscosity and thermal conductivity of the xenon gas are extrapolated from lower temperature data. The viscosity and thermal conductivity for Flibe vapor are calculated directly from the kinetic theory of gases and are not based on experimental measurements. The gas densities are only approximate. For SOMBRERO, the density may be a factor of two lower. In any case, the heat fluxes to both targets are dominated by radiation. The

SOMBRERO conditions are worse by an order of magnitude because of the higher temperature of the first wall.

**Table 4.11. Target Heat Loads**

	<b>SOMBRERO</b>	<b>Osiris</b>
Wall Temperature (K)	1758	923
Gas Temperature (K)	1758	923
Gas Density (cm <sup>-3</sup> )	$3.55 \times 10^{16}$	$3.55 \times 10^{12}$
Gas Species	Xenon	Flibe
Gas Mass Density (μg/cm <sup>3</sup> )	7.79	$8.38 \times 10^{-5}$
Target Speed (m/s)	200	150
Target Diameter (cm)	0.6	0.6
Gas Viscosity (μPoise)	900	0.022
Reynolds Number	107	29.2
Gas Conductivity (W/cm-K)	$2.45 \times 10^{-4}$	$0.13 \times 10^{-7}$
Surface Conductance (W/cm <sup>2</sup> -K)	$2.42 \times 10^{-3}$	$5.85 \times 10^{-8}$
Conductive Heat Load (W/cm <sup>2</sup> )	4.2	$6 \times 10^{-5}$
Radiative Heat Load (W/cm <sup>2</sup> )	54.2	4.12
Total Heat Load (W/cm <sup>2</sup> )	58.4	4.12

### 4.3.2 PELLET Computer Code

The PELLET computer code was developed at the University of Wisconsin to simulate the heating of ICF targets by the target chamber environment. PELLET uses information on the target geometry and the surface heat load to calculate the temperature at every position in the target as a function of time. In this section we will describe the numerical method used and the thermal properties used in these calculations.

#### 4.3.2.1 Numerical Method

PELLET is a one-dimensional finite-difference computer code. A one dimensional mesh is defined in slab geometry. Therefore, this code is accurate only for targets where the material is thin compared to its radius, which is true for all reasonable targets. Heat transfer inside the central cavity void is not considered. Heat is deposited at the outer surface only and diffuses into the target as predicted by the standard temperature diffusion equation,

$$\frac{\partial T}{\partial t} = \frac{1}{C_p} \left[ \nabla \cdot \chi \Delta T + Q \right]$$

Here,  $C_p$  is the specific heat of the target material, and  $\chi$  is the conductivity. Both are functions of temperature.  $Q$  is an energy source which is a function of position and time.  $T$  is the material temperature.

We have used an implicit differencing scheme<sup>4.21</sup> to solve the temperature diffusion equation. We have used the Crank-Nicholson method,<sup>4.22</sup> which is always numerically stable, to advance the time step. To achieve reasonable accuracy, we use time steps,  $\Delta t$ , that obey the condition,

$$\Delta t \leq \frac{(\Delta x)^2}{2\sigma}$$

Here,  $\sigma = \chi/C_p$  is the thermal diffusivity, and  $\Delta x$  is the width of a spatial zone. This is required because  $\chi$  and  $C_p$  are strong functions of temperature in the cryogenic regime. A zero heat flux boundary condition is applied at the inside edge of the innermost zone and a time-dependent heat flux equal to  $Q(t)$  is imposed at the outer edge of the outermost zone.

#### 4.3.2.2 Thermal Properties

Temperature dependent thermal properties are used in these target heating calculations. We have used reported values for thermal properties.<sup>4.23,4.24</sup> For example, the thermal conductivity and specific heat for polystyrene from the first reference are shown in Figs. 4.18 and 4.19, respectively. One can clearly see the strong temperature dependence in these properties. The plastic parts of the targets present the greatest barrier to heat diffusion. We have chosen the properties of polystyrene as representative for the plastic in actual targets. Thermal conductivities for solid hydrogen are shown in Fig. 4.20. Several curves are shown, reflecting different concentrations of molecular spin state  $J = 1$  in the diatomic hydrogen molecules. The  $J = 1$  state hydrogen molecules are very effective in reducing heat flow because they have a larger phonon cross-section. Souers has recommended using the  $H_2$  curve with a  $J = 1$  concentration of 0.70 for DT.<sup>4.23</sup> The specific heat of DT is shown in Fig. 4.21. Temperature dependent thermal properties of lead (not shown here) were also used in the calculations.

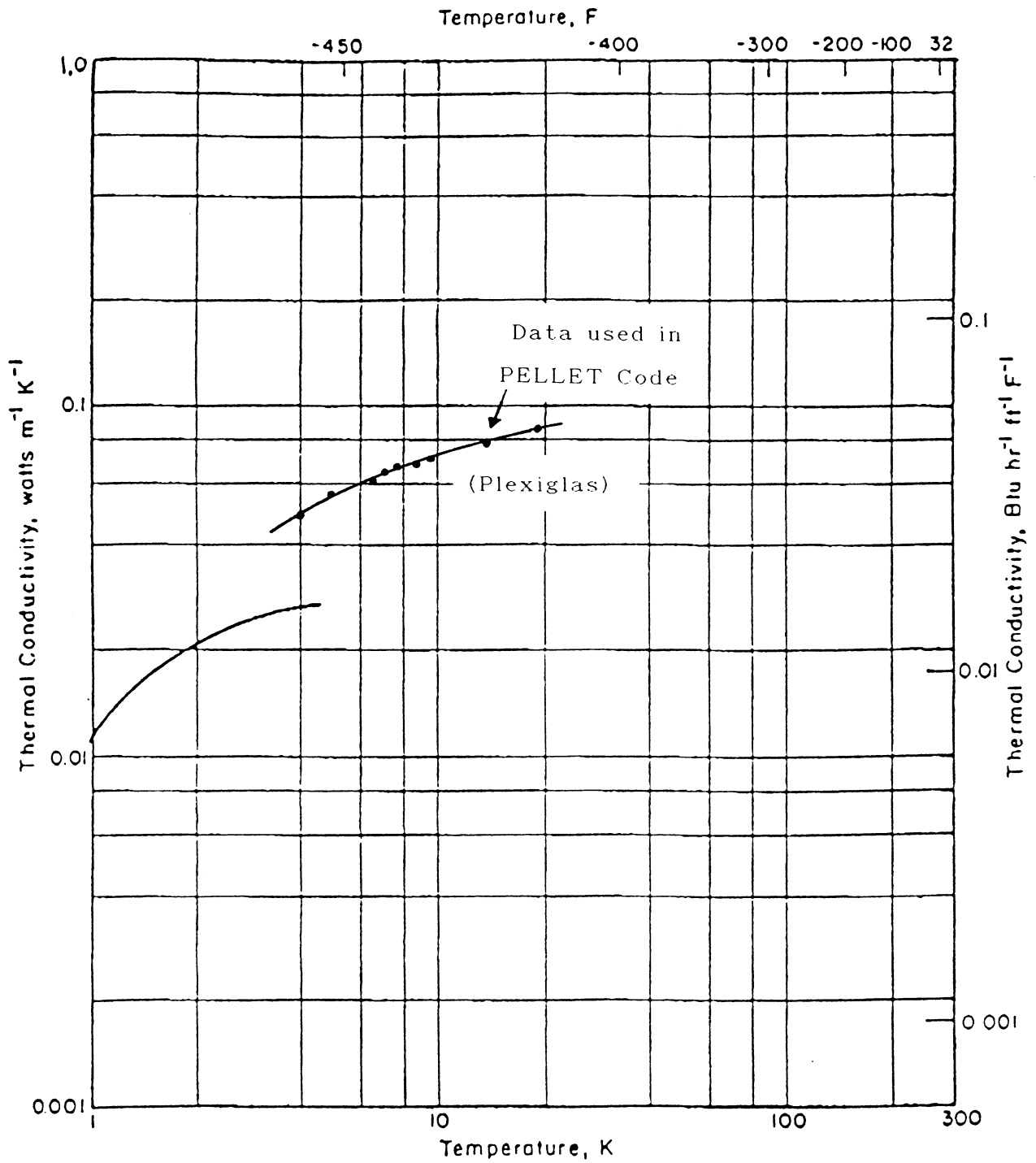


Fig. 4.18. Thermal conductivity of polystyrene.<sup>4.23</sup>

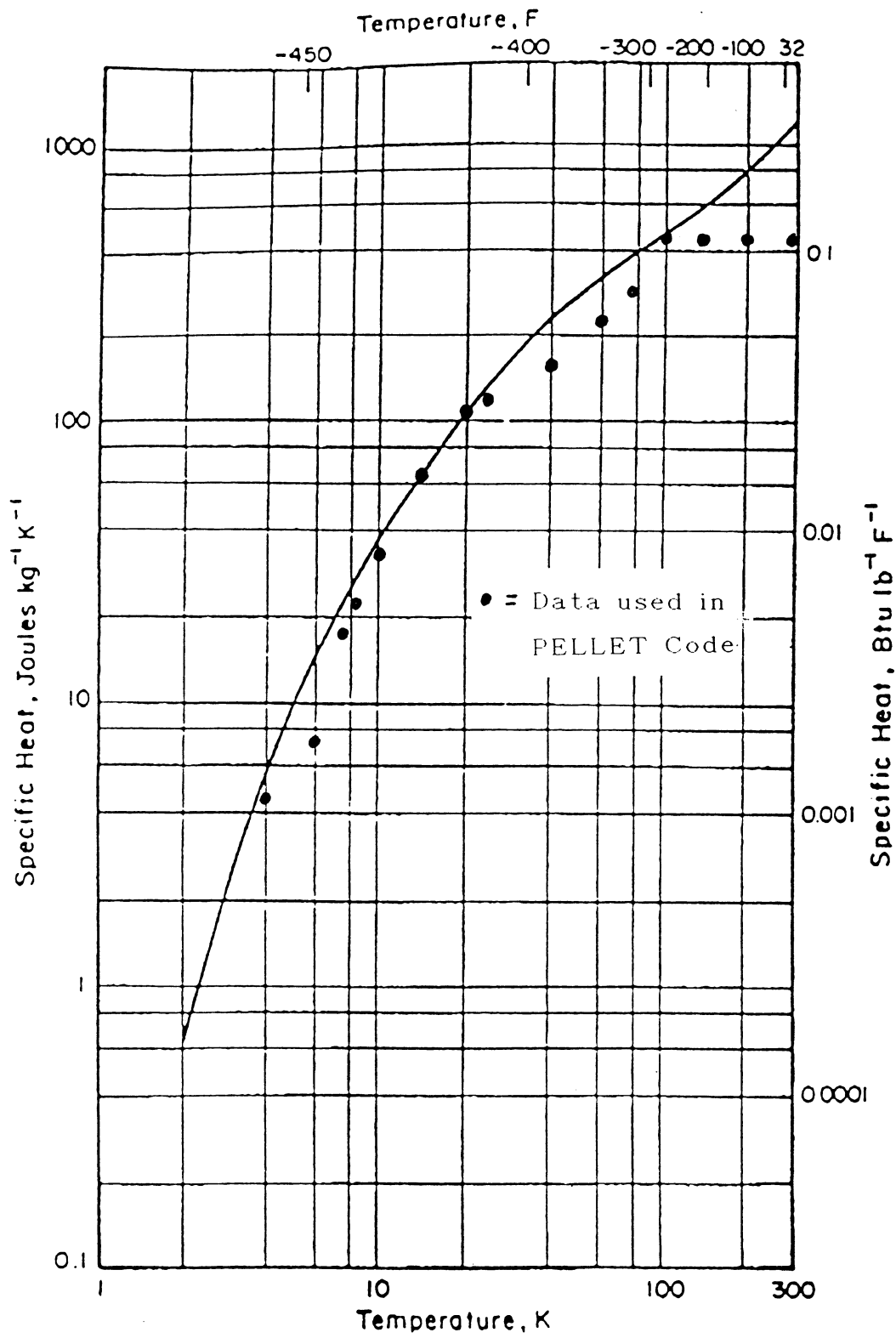


Fig. 4.19. Specific heat of polystyrene.<sup>4.23</sup>

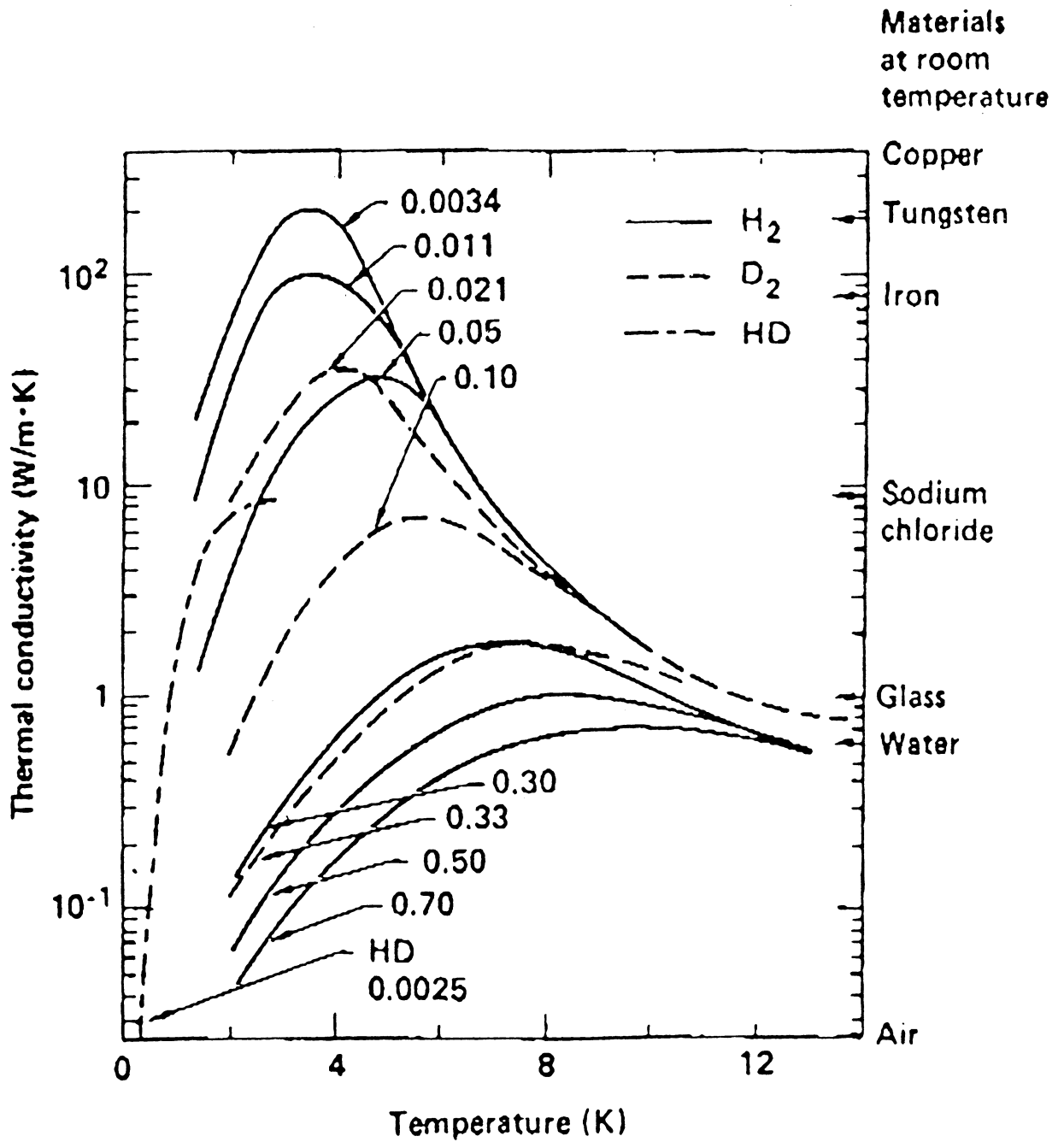


Fig. 4.20. Thermal conductivity of solid H<sub>2</sub>, HD, and D<sub>2</sub> as a function of temperature for different J = 1 concentrations.<sup>4.24</sup>

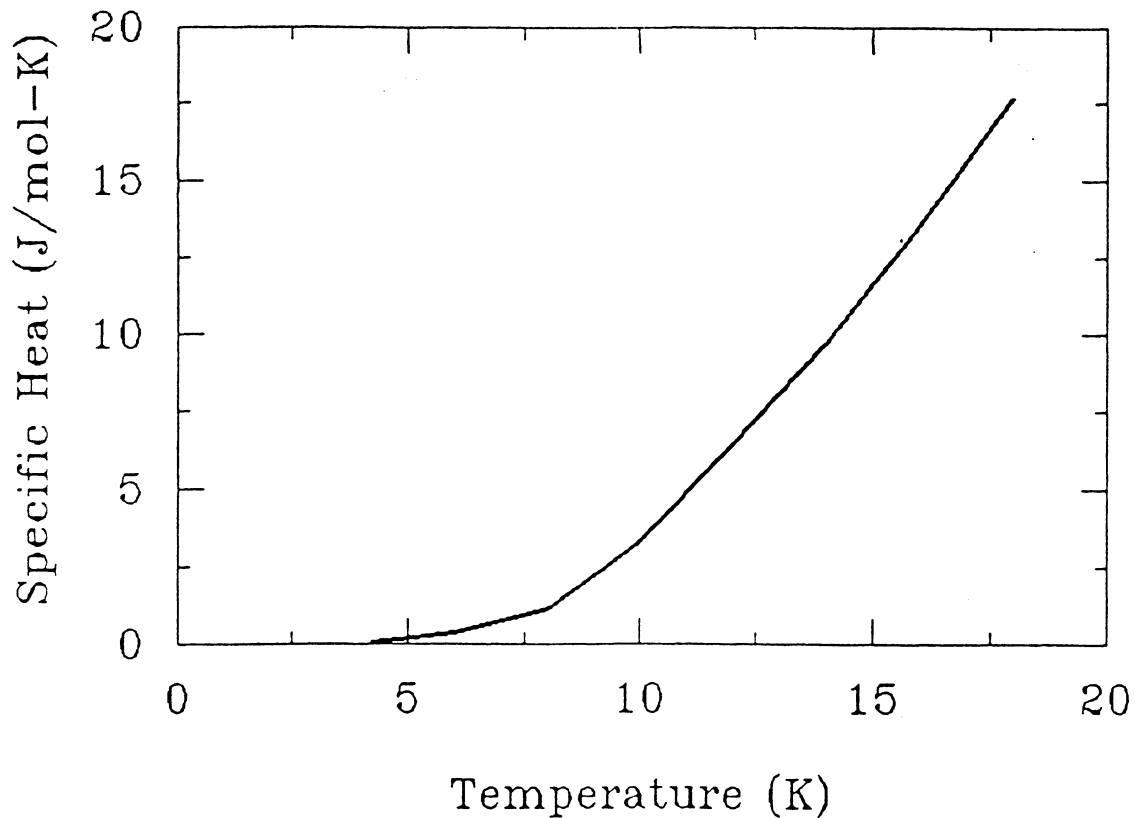


Fig. 4.21. Specific heat of DT.<sup>4.24</sup>

### 4.3.3 Target Heating Results

We have used the PELLET code to calculate the temperatures in the targets parametrically for a number of different heat loads. Estimates of the heat loads for both reactor designs are discussed in an earlier section. In all cases, we assumed that the whole target was initially at 4 K and have, therefore, assumed that  $\beta$  decay heating of the fuel during storage has been accommodated by appropriate cooling.

#### 4.3.3.1 Heavy Ion Target

The results of PELLET calculations for the Osiris target design are shown in Figs. 4.22 through 4.24. Figure 4.22 shows temperature profiles in the target material at various times for the case of a heat load of  $2 \text{ W/cm}^2$ . While this is lower than the  $4 \text{ W/cm}^2$  calculated in

Table 4.11, one sees that the steepest temperature drop occurs in the plastic shell, indicating that the plastic is the most important impediment to heating of the fuel. The lead and the DT have flat temperature profiles because they both have high thermal diffusivity. If the target must travel  $\sim 5$  m through the chamber and is injected at a velocity of 150 m/s,  $\sim 33$  ms will be required for the target to reach the ignition point. From Fig 4.22, one sees that for this heat load, the fuel would only reach about 7 K by this time. Figures 4.23 and 4.24 show the temperature versus time at the outer and inner edges of the fuel, respectively, for a variety of heat loads. These show that even at a heat load of  $500 \text{ W/cm}^2$ , the fuel temperatures would be well below the triple point at 33 ms.

#### 4.3.3.2 Laser Target

The results of PELLET calculations for the SOMBRERO target design are shown in Figs. 4.25 through 4.27. Temperature profiles in the SOMBRERO target at various times are shown in Fig. 4.25 for a constant heat flux of  $50 \text{ W/cm}^2$  (slightly less than the estimated  $58 \text{ W/cm}^2$ ). Note the substantial temperature drop across the plastic shell. Once again, the thermal diffusivity of the plastic provides thermal protection for the fuel. The temperatures at the outer and inner edges of the DT fuel are plotted as a function of time in Figs. 4.26 and 4.27, respectively, for a variety of heat loads. If the targets must travel 6.5 m through the chamber before it is imploded and if the targets travel at 200 m/s, the target surface is heated for 33 ms. From these two figures, one can see that for a heat load of  $58 \text{ W/cm}^2$  the temperature at the outer and inner edges of the fuel at 33 ms is 13 K and 10 K, respectively. This is still well below the DT triple point. The 200 m/s target velocity was assumed before the final target injector design point of 151 m/s was chosen (see Section 4.2). If the targets are only accelerated to 151 m/s, the heat load, which is dominated by radiation, will not be reduced much, but the time that the target experiences the heat load would increase to 43 ms. Extrapolating the curves to this time, we estimate the outer and inner fuel temperatures to be  $\sim 17$  K and 11 K, respectively. This is still below the triple-point, but there is only a 4 K margin for error.

While the fuel remains below the triple point, the outer surface temperature of the polystyrene capsule is  $\sim 700$  K (see Fig. 4.25). Since this is well above the melting point of polystyrene, it will be necessary to protect the capsule during transit through the chamber. One possibility is to keep the capsule in the sabot for most of the transit time. Another option is to freeze a thin layer of inert gas (e.g., Xenon) on the outer surface of the capsule. The frozen gas would act as a sacrificial heat sink and evaporate as the capsule transits the chamber. This could reduce the time that the bare capsule is exposed to the hot chamber to a few ms. Clearly, this is an area that requires further investigation.

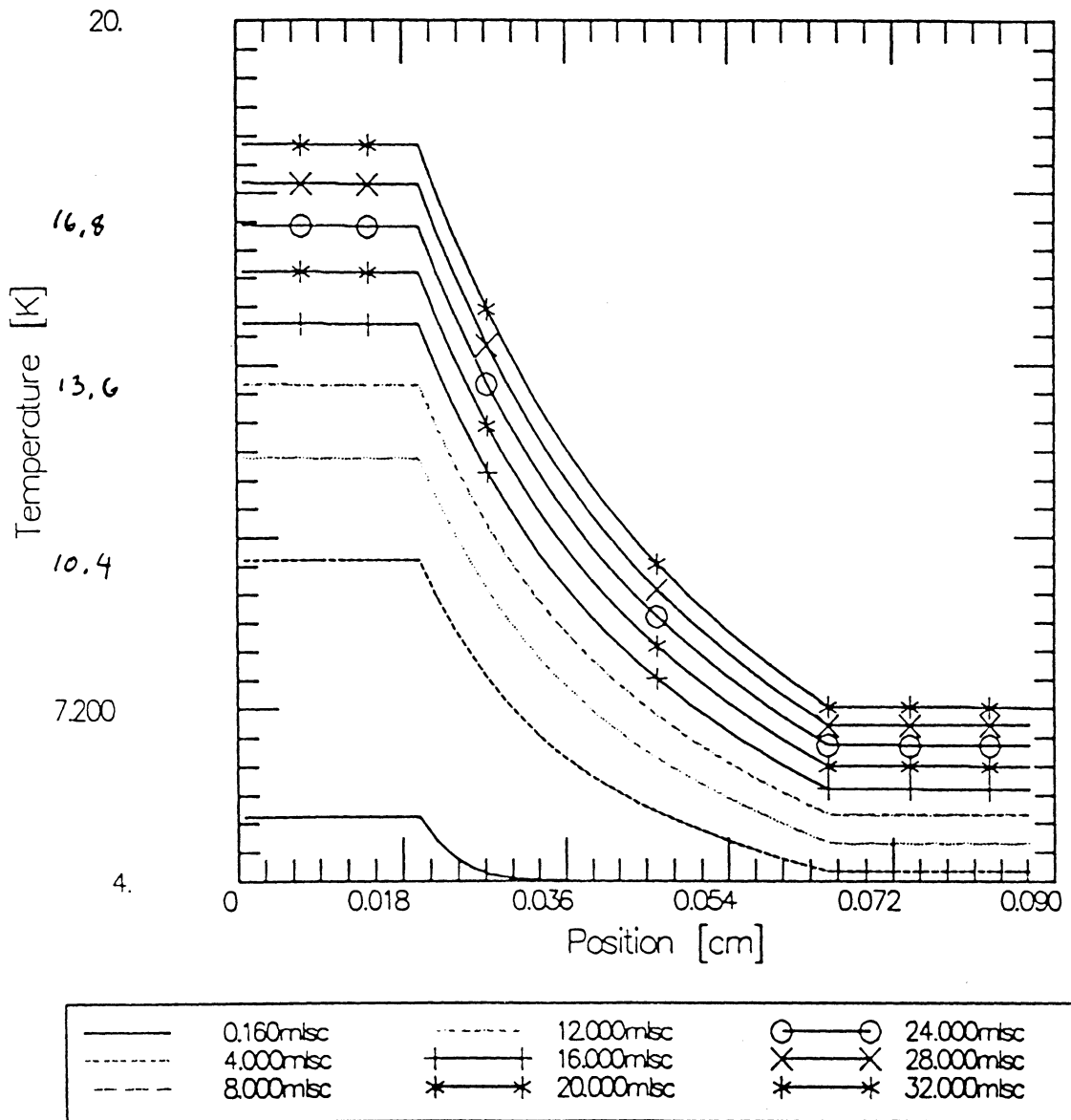
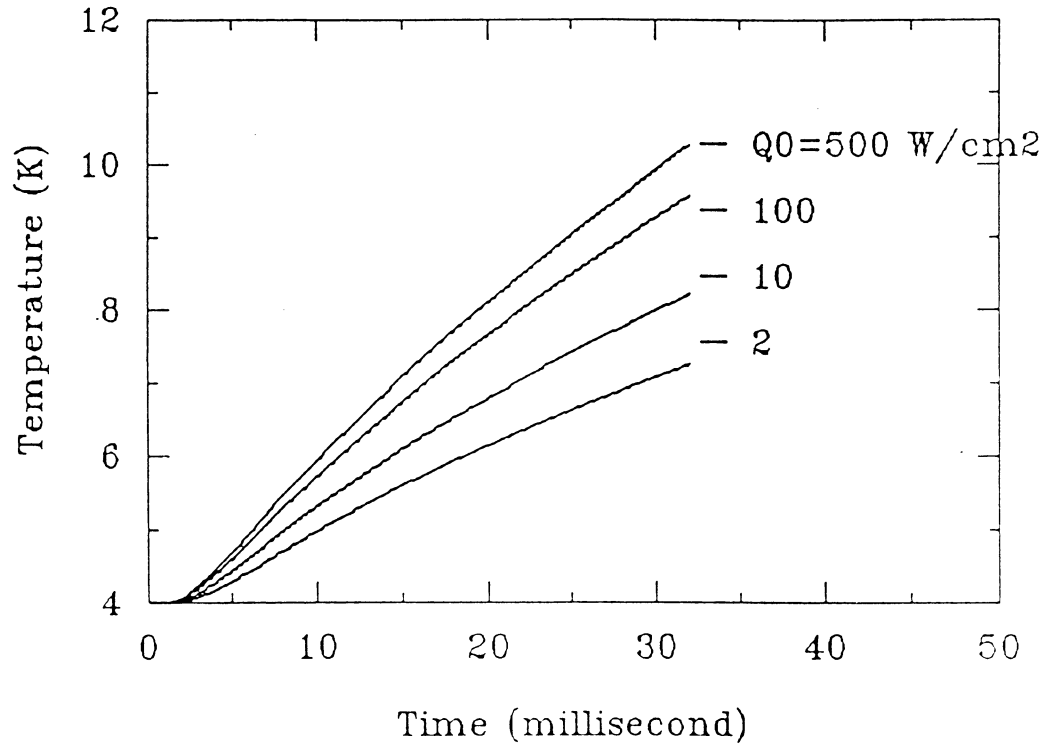
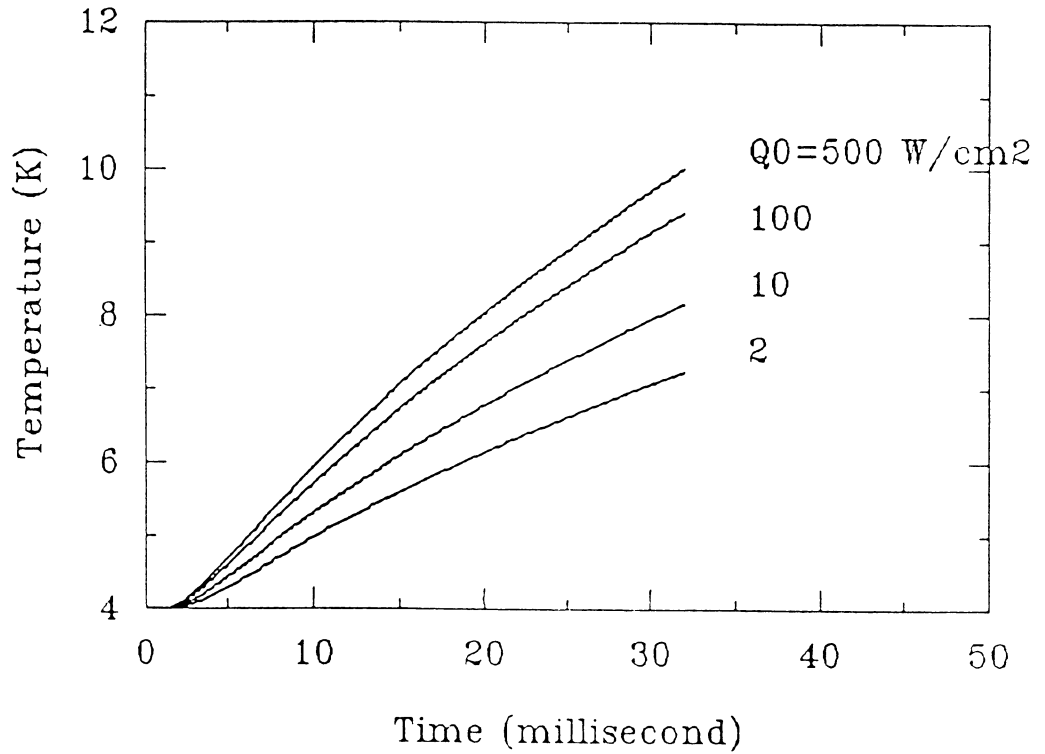


Fig. 4.22. Target material temperatures versus distance from outer edge of target at several times for the Osiris target. The surface heat flux is  $2 \text{ W/cm}^2$ .



**Fig. 4.23.** Temperature at the outside edge of the fuel in the Osiris target versus time for several surface heat fluxes.



**Fig. 4.24.** Temperature at the inside edge of the fuel in the Osiris target versus time for several surface heat fluxes.

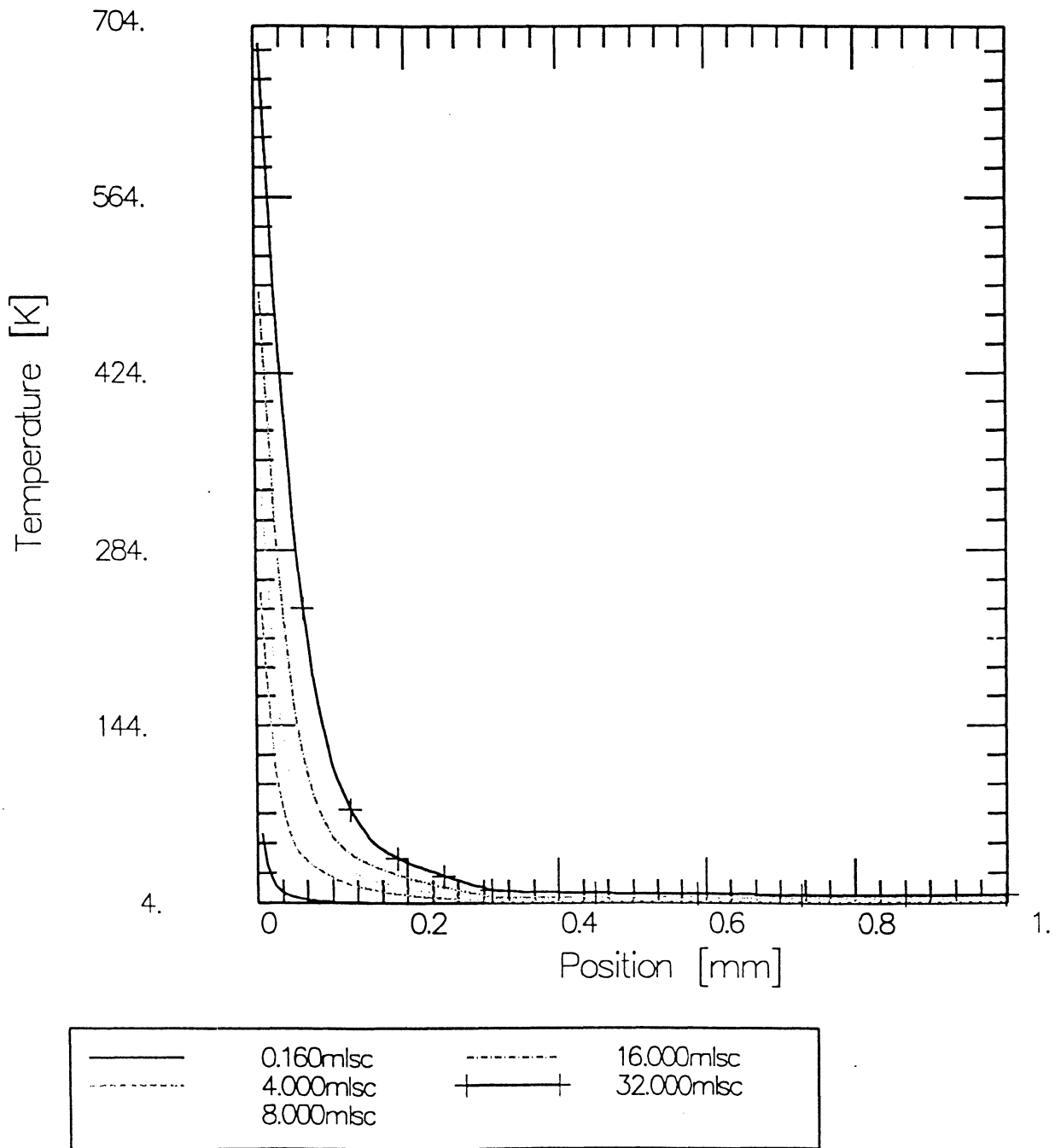
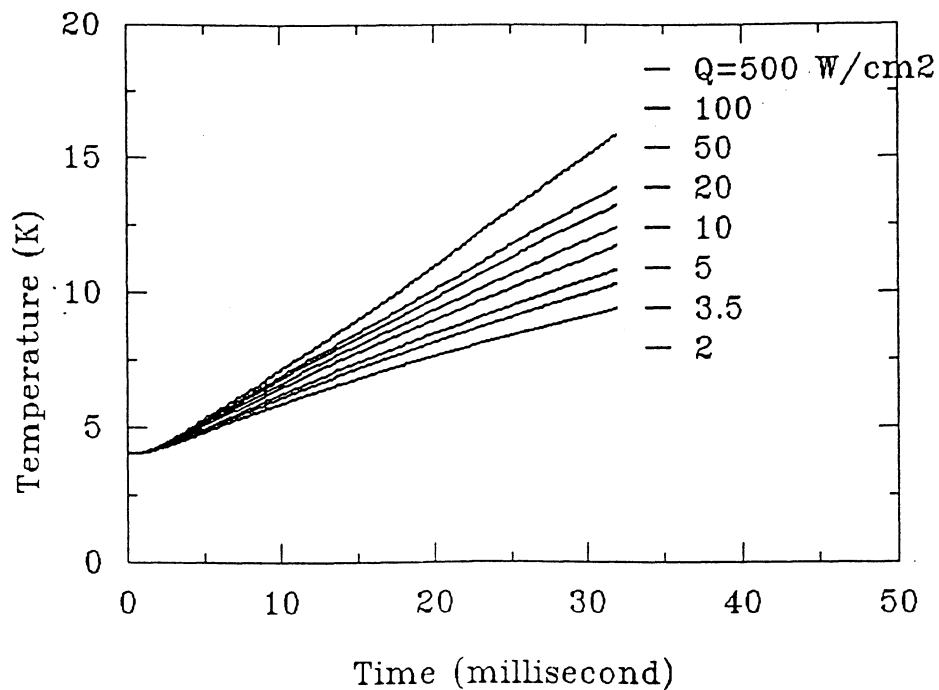
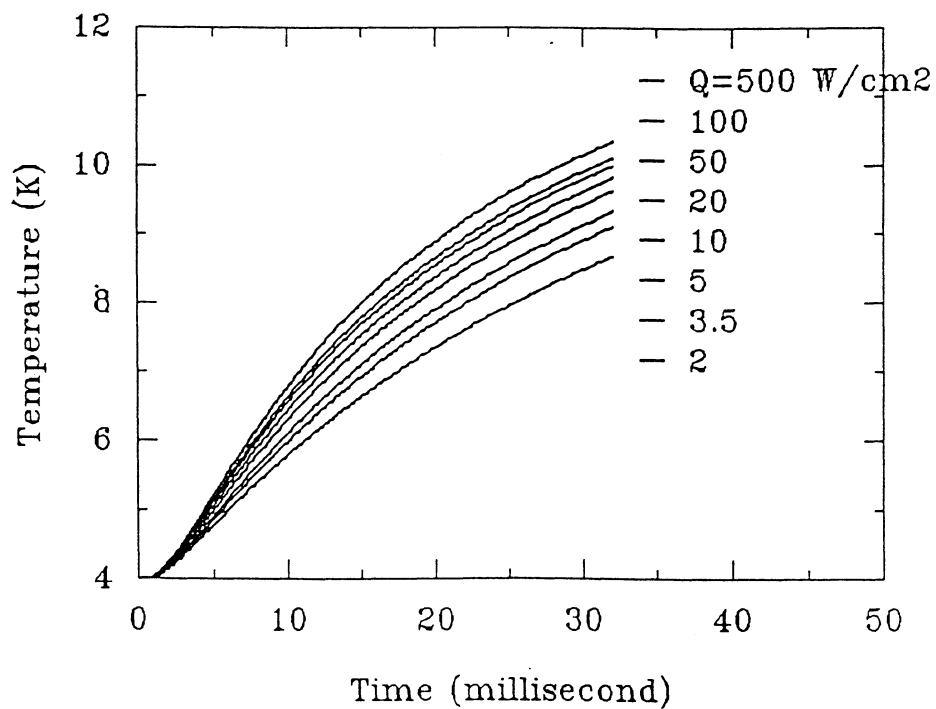


Fig. 4.25. Target material temperatures versus distance from outer edge of target at several times for the SOMBRERO target. The surface heat flux is 50 W/cm<sup>2</sup>.



**Fig. 4.26.** Temperature at the outside edge of the fuel in the SOMBRERO target versus time for several surface heat fluxes.



**Fig. 4.27.** Temperature at the inside edge of the fuel in the SOMBRERO target versus time for several surface heat fluxes.

#### 4.4 REFERENCES FOR CHAPTER 4

- 4.1 C.D. Hendricks, "Production of Thin Wall Small Diameter Polystyrene Shells," American Association for Aerosol Research, Annual Meeting, Seattle, WA, Paper 15A (Sept. 14-17, 1987).
- 4.2 C.D. Hendricks, "Hollow Glass Sphere Production," Lawrence Livermore National Laboratory Laser Program Annual Report, UCRL-50021-76, 4 (1976).
- 4.3 U. Kubo et al., ILE Osaka University, ILE-APZ-79, 177 (1979).
- 4.4 C.D. Hendricks, C.A. Foster, "Hollow Hydrogen Shells for Laser Fusion Targets," American Physics Society Series II, **19**, 927 (Oct. 1974).
- 4.5 C.D. Hendricks, C.A. Foster, "Hollow Hydrogen Shells for Laser Fusion Targets," *Applied Physics Letters*, **26**, 580 (May 15, 1975).
- 4.6 J.F. Miller, "A New Method for Producing Cryogenic Laser Fusion Targets," *Advancements in Cryogenic Engineering*, **23** (1978).
- 4.7 C.D. Hendricks, et al., "A New Technique for Fabricating Cryogenic Laser Fusion Targets Using Cold-gas Jets," *Applied Physics Letters*, **34**, 282 (Feb. 15, 1979).
- 4.8 J.D. Simpson, J.K. Hoffer, and L.R. Foreman, "Beta-Layering of Solid Deuterium-Tritium in a Spherical Polycarbonate Shell," *Fusion Technology*, **21**, 330 (1992).
- 4.9 H. Rieger et al., "Cryogenic Laser Target Fabrication System Directly Operable Inside a Target Chamber," Lawrence Livermore National Laboratory, UCRL-83079 (1979).
- 4.10 S.L. Milora, "Review of Pellet Fueling," *Journal of Fusion Energy*, **1**, 15 (1981).
- 4.11 S.L. Milora and C.A. Foster, *Rev. Sci. Instrum.*, **50**, 482 (1979).
- 4.12 C.A. Foster and S.L. Milora, "ORNL Pellet Acceleration Program," *Proc. Fusion Fueling Workshop*, Princeton N.J., DOE CONF-771129, 117 (1978).
- 4.13 R. Kreutz, "Pellet Delivery for the Conceptual Inertial Fusion Reactor HIBALL," *Fusion Technol.*, **8**, 2708 (Nov. 1985).
- 4.14 J. Woodworth, Lawrence Livermore National Laboratory, Personal Communication (Jan. 1991).
- 4.15 P. Kevin, et al., "Relay Mirror Experiment / Wideband Angular Vibration Experiment," Phillips Laboratory, PL-TR-91-1088, **1**, (1992).
- 4.16 "Airborne Laser Laboratory," Kirkland AFB, AFWL-TR-8C, Vol. I-IV (1988).
- 4.17 M.J. Monlser, "Laser Fusion: An Assessment of Pellet Injection, Tracking and Beam Pointing," *Proc. 3rd Topical Meeting on the Technology of Controlled Nuclear Fusion*, Santa Fe, New Mexico, (May 1978).
- 4.18 M.R. Lee and J. Sesak, "Control System Requirement Extracted from the Stanlab Hardware Specification, EM-238," Lockheed Missiles and Space co., F185873 (1988).

- 4.19 "The University of Rochester Laboratory for Laser Energetics, Annual Report, 1 October 1984 - 30 September 1985," DOE/DP/4020-05, 126 (Jan. 1986).
- 4.20 R.O. Bangerter, J. W.-K. Mark, and G. Magelssen, "Simple Target Models for Ion Beam Fusion Studies," LLNL Report, UCID-20578 (1985).
- 4.21 R.D. Richtmeyer and K.W. Morton, "Difference Methods for Initial-Value Problems," Interscience Publishers, New York, (1967).
- 4.22 J. Crank and P. Nicholson, "A Practical Method for Numerical Integration of Solutions of Partial Differential Equations of Heat-Conduction Type," *Proc. Cambridge Philos. Soc.*, **43**, 50 (1947).
- 4.23 "Handbook on Materials for Superconducting Machinery," Metals and Ceramics Information Center, Battelle Columbus Laboratories Report (1977).
- 4.24 P.C. Souers, "Hydrogen Properties for Fusion Energy," Univ. of California Press, Berkeley, CA (1986).